IOP Publishing Superconductor Science and Technology
Supercond. Sci. Technol. 29 (2016) 075002 (12pp) doi:10.1088/0953-2048/29/7/075002

Vibration effect on magnetization and critical current density of superconductors

Igor A Golovchanskiy[1,2,3], Alexey V Pan[1,4], Jonathan George[1], Frederick S Wells[1], Sergey A Fedoseev[1,5] and Anatoly Rozenfeld[5]

[1] Institute for Superconducting and Electronic Materials, University of Wollongong, Northfields Avenue, Wollongong, NSW 2522, Australia
[2] Moscow Institute of Physics and Technology, State University, 9 Institutskiy per., Dolgoprudny, Moscow Region, 141700, Russian Federation
[3] Laboratory of Superconducting Metamaterials, National University of Science and Technology MISIS, 4 Leninsky prosp., Moscow, 119049, Russian Federation
[4] National Research Nuclear University MEPhI (Moscow Engineering Physics Institute), 31 Kashirskoye Shosse, 115409, Moscow, Russian Federation
[5] Centre for Medical Radiation Physics, University of Wollongong, Northfields Avenue, Wollongong, NSW 2522, Australia

E-mail: pan@uow.edu.au

Received 12 April 2016, revised 27 April 2016
Accepted for publication 4 May 2016
Published 17 May 2016

Abstract

In this work the effect of vibrations on critical current density (J_c) of superconductors has been studied. The vibrations are shown to affect J_c of all types of superconductors during their measurements, employing a vibrating sample magnetometer (VSM). Increasing vibration frequency (f) and/or amplitude (A) leads to progressive reduction of J_c as a function of magnetic field (B_a). The effect of vibrations is substantially stronger in thin films. It leads to development of unexpected kinks on $J_c(B_a)$ curves. Analysis of magnetization loops and relaxation of magnetization in YBCO films revealed that the vibration effect can be treated as the effective reduction of pinning potential. The asymmetry of the vibration effect in ascending and descending B_a is observed, indicating differences in free energy of the corresponding vortex structures. Thermal effects induced by vibrations with large f and A are shown to have rather insignificant influence, while the vibrational vortex dynamics exhibit a strong impact. The irreversibility field (B_{irr}) is shown to be instrumentally defined, and its value depends on VSM settings. In addition, the practical importance of B_{irr} for J_c modeling is demonstrated.

Keywords: superconductors, vortex pinning, critical current density, vibration, vortex dynamics, irreversibility field

(Some figures may appear in colour only in the online journal)

1. Introduction

The behavior of superconductors exposed to electromagnetic fields at different frequencies by placing the superconductors in these fields [1–12] or by mechanical oscillations of these superconductors in a constant DC field [13–15] has been well documented. The superconducting response to frequencies varies significantly. The *enhancement* of irreversible magnetization has been reported in frequencies starting from 20 Hz [1] up to the depinning frequency [2–4] as a result of increasing immobility of vortices. The onset of energy dissipation above the depinning frequency [5] was explained within the mean-field model [6]. The shift of the irreversibility line in type-II superconductors [7, 9] due to enhanced relaxation of drifting vortices [11] has explained different vortex phase transitions [8, 10]. Superconductors vibrating with kilohertz frequencies in DC magnetic fields have been used to investigate a range of superconducting properties from Meissner states to melting transitions [13], superconducting sheath vortex transitions and two co-existing orthogonal vortex lattices [14, 15]. In addition,

superconducting films moving in inhomogeneous magnetic/temperature environments shed light on the origin of the so-called paramagnetic 'Meissner' (magnetization) effect [16].

In this work, we study the lowest frequency range investigated to-date, which is relevant to applications of rotating superconducting systems, such as motors, flywheels, power generators (e.g., windmills), etc. We show unexpectedly dramatic influence on the behavior of different superconductors, which is at odds with any enhancements observed in [1–4], but is somewhat similar to the observed shift of the irreversibility line in [8, 9, 16], while exhibiting unexpected, vibration driven vortex dynamics.

We employ vibration sample magnetometry (VSM)[17], which is one of the most common approaches for determination of current-carrying capabilities of superconductors. Generally, if standard measurements of physical properties are carried out, it is expected that all parameters involved in the measurements have clear designation and well-defined influence. However, this is not the case for magnetization measurements employing VSM. In [18], a strong deviation of the critical current density dependence on the applied magnetic field ($J_c(B_a)$) by orders of magnitude was demonstrated in YBCO thin films as the result of variation of the never-discussed parameters of the measurements: vibration frequency (f) and amplitude (A). It appears that inconsistencies with VSM measured $J_c(B_a)$ have been known, attributed to differences in the corresponding electric field criterion (E_{cr}) used in VSM and other measurement techniques, such as transport current measurements [19, 20]. An obvious shift between $J_c(E)$ curves obtained by VSM PPMS measurements and transport current measurements can be seen in figures 10, 11 and 15 of [19]. The origin of such inconsistencies remains unexplained so far.

Suppression of $J_c(B_a)$ by vibrations implies that the fundamental link $E_{cr} - B_a - J_c$ seems to fail for VSM. Indeed, up to now these measurements ignore the influence of vibrations (physical movement of a sample), which leads to wrong estimation of pinning properties [21] and irreversibility fields [18] of superconductors. The origin of this problem has never been discussed in the literature, instead some conclusions have been made on the basis of incorrectly interpreted results (for some examples, see [21]). However, the $J_c(B_a)$ obtained by VSM seems to regain its meaningfulness by minimizing vibration influence with $f \to 0$ and $A \to 0$ [18].

Hence, in this work, we experimentally study the vibration effect on superconducting current-carrying capabilities in different superconductors and the origin of this effect. It would allow eliminating existing inconsistencies in measurements, corresponding data interpretations, and verifying models and explanations proposed on the basis of results obtained with instrumentally driven, phenomenological artefacts. The understanding of this influence can also allow one to study possible suppression of superconducting properties by vibrations at low frequency/amplitude, which naturally appears during application of superconductors [22–25].

First, the effect of vibration on various superconducting materials with different pinning properties, geometry, and at different temperatures is discussed for thin films and bulk samples in section 3. In section 4, more detailed study of vibration effect on magnetization and relaxation of magnetization of YBCO thin films is presented. The $J_a(B_a)$ scaling by the magnetic field sweep rate and the frequency of vibrations is demonstrated in section 5. In section 6, a convenient way to characterize the vibration effect through the irreversibility field is explored. It is shown that the irreversibility field dependence on VSM settings is a good representation of vibration effect on the entire $J_c(B_a)$ curve. Finally, the possible origin of the vibration influence is discussed in section 7.

2. Experimental details

YBCO thin film of 300 nm thickness was produced on 5 × 5 mm^2 size $SrTiO_3$ single crystal substrate using standard pulsed-laser deposition (PLD) method [26]. Deposition was performed by KrF excimer laser with wavelength of 248 nm at 2 Hz repetition rate. The PLD chamber was pre-evacuated down to 10^{-6} mBar. During the deposition, the substrate temperature and back oxygen pressure were 780 °C and 400 × 10^{-3} mBar, respectively. The thin films had critical temperature $T_c \simeq 89.5 \pm 0.5$ K as measured by DC magnetic measurements in MPMS at $B_a = 2.5$ mT.

Nb-1 thin film of 450 nm thickness with $T_c = 8.4 \pm 0.1$ K was produced by magnetron sputtering from N4 purity Nb target on the same $SrTiO_3$ substrate. The back pressure in the deposition chamber was ~10^{-9} mBar. During the deposition, the substrate temperature and back argon pressure were 350 °C and 6.5 × 10^{-3} mBar, respectively. Nb-2 film of 450 nm thickness with $T_c = 8.9 \pm 0.1$ K was produced in the same magnetron sputtering system with substrate temperature 500 °C during deposition.

MgB_2 bulk sample was fabricated using *in situ* reaction technique by Shcherbakova *et al* as described in [27–29]. The dimensions of the sample are 1 × 2 × 3 mm^3.

Nb bulk sample was cut from the N4 purity Nb bulk target employed for the magnetron sputtering of Nb thin films in this work. The dimensions of this Nb sample are ~2 × 3 × 5 mm^3.

Magnetization measurements were performed by Quantum Design VSM PPMS, employing various frequencies and amplitudes of VSM. The majority of the measurements were performed with magnetic field sweep rate $dB_a/dt = 5 \times 10^{-3}$ T s^{-1} unless specified otherwise. The magnetic field was applied in the out-of-plane direction for the thin films and along the longest dimension for the bulk samples. The critical current density was determined from magnetization measurements using the Bean formula for rectangular samples [30].

3. Influence of vibrations on J_c of various superconducting materials

3.1. Thin films

In figure 1, the $J_c(B_a)$ dependences of the YBCO thin film are plotted, which are measured by VSM PPMS at 77 K for different f and A. The curves measured at the lowest frequency

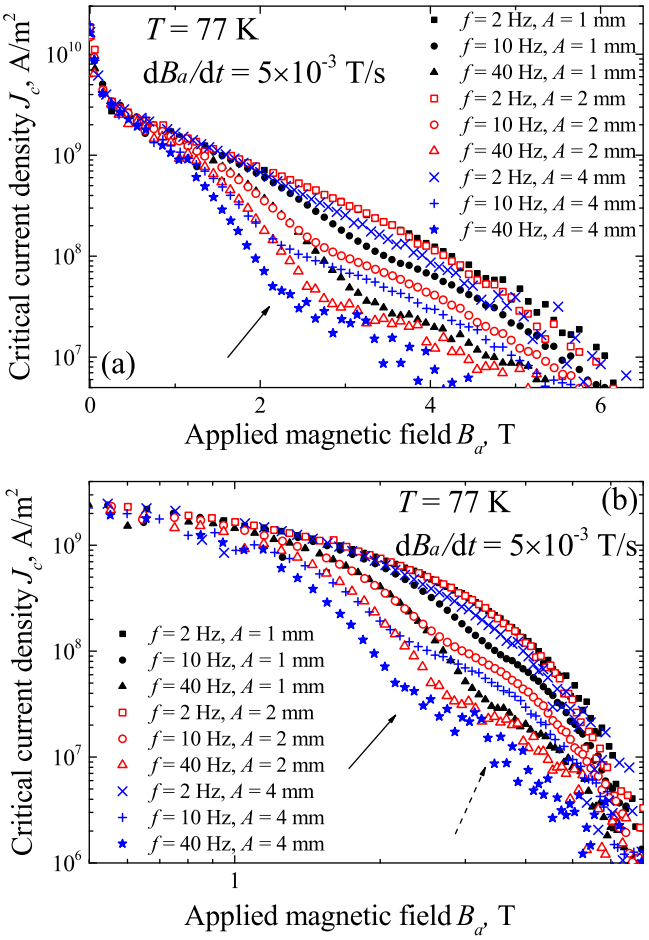

Figure 1. Critical current density dependences on magnetic field of YBCO thin film at $T = 77$ K measured at $dB_a/dt = 5 \times 10^{-3}$ T s^{-1} and different f and A, shown in semi-log (a) and log-log (b) scale. Arrows indicate kinks on $J_c(B_a)$ curves.

($f = 2$ Hz) and amplitude ($A = 1$ mm) represent the $J_c(B_a)$ behavior, which would be expected from these measurements if only the sweep rate defining the corresponding electric field criterion ($E_{cr} \sim dB_a/dt$) was taken into account [18]. This behavior determined by E_{cr}, which can be easily scaled and compared to the behavior measured by transport current measurements [18, 21], we attribute to the *undisturbed* vortex state/motion by the additional influence of high vibrational frequency and its amplitude. Sample vibration with enhanced f and/or A leads to the J_c degradation, which enhances with increasing f, A and B_a. The effect of the sample vibration on the $J_c(B_a)$ becomes noticeable at $B_a > 0.5$ T. Note at this field, the critical current density is already dropped by approximately one order of magnitude relative to its zero field value [$J_c(B_a = 0.5$ T$)/J_c(0) \sim 10^{-1}$]. The J_c degradation developed by the influence of vibration parameters relative to the *undisturbed* state reaches the maximum factor of ~40 for the curve measured with the highest f and A available at $B_a \sim 2$ T, where a kink in this curve is also measured.

The kink (shown by the solid arrows in figures 1(a, b)), being the characteristic feature of all $J_c(B_a)$ curves measured with substantial frequency ($f > 3$ Hz). It appears at $B_a \sim 2$ T (or higher, depending on the parameters of the measurements), and is likely to indicate some transition in vortex state/motion. The position of the kink on the J_c-axis mostly depends on f, while the position on the B_a-axis is primarily determined by A.

At higher magnetic fields there is a second, less pronounced kink in $J_c(B_a)$ dependence shown by the dotted arrow in figure 1(b), and the best visible for $J_c(B_a)$ measured at $f = 10$ Hz. To the best of our knowledge, the existence of this kind of feature in $J_c(B_a)$ curves of typical YBCO films has never been reported or considered. The nature of these kinks is as yet unknown.

The frequency of VSM can vary in a range of 1 to 60 Hz. Obviously, the $J_c(B_a)$ curves degrade more rapidly at $f > 10$ Hz, developing the kink (see in figure 4 of [18]). The default VSM settings are $f = 40$ Hz and $A = 2$ mm, which obviously develop the kink and are described by a lower E_{cr} than the one expected from the sweep rate dB_a/dt set experimentally. If the sample measured is rather tiny, the measured magnetization signal ($M \propto J_c$) may be very small above the kink. Hence, it can lead to wrong interpretations for the part of the $J_c(B_a)$ curve above the kink to simply be, for example, noise.

In general, the smallness of the M-signal would strongly affect the definition of B_{irr}, which would lose its designation to determine the loss of vortex pinning. In this work, we define the irreversibility field (B_{irr}) from $J_c(B_a)$ graphs at the intersection of a corresponding $J_c(B_a)$ curve with the line indicating the lowest J_c value plotted in the corresponding graph. This value is different for different samples types due to their different sizes, measurement temperatures, pinning strength, etc.

We should also note that we have measured the influence of different frequencies on $J_c(B_a)$ of YBCO films at different temperatures including as low as, e.g. 10 K. At $T = 10$ K, B_a was applied up to 10 T with no visible effect of vibrations detected. However, at this temperature it was not possible even to approach to B_{irr} of YBCO thin films, because at $T = 10$ K it can reach up to ~100 T [19, 31, 32]. According to figure 1, the effect of vibrations is visible upon approaching to the irreversibility field. Hence, it was not possible to measure the influence of vibrations at $T = 10$ K.

In figure 2 $J_c(B_a)$ curves for the Nb-1 thin film measured with different f and A at $T = 4.2$ K are shown. Note that the Nb-1 film has the same geometry as the YBCO film, but it has a different nature of pinning. Except the low field (<1.5 T) flux-jump region (which does not correspond to a critical state of the superconductor), the effect of sample vibrations on $J_c(B_a)$ in Nb-1 film is similar to that of the YBCO film as follows: (i) The effect becomes evident at $B_a > 0.5$ T where J_c remains of the same order as at zero field (note, that the effect of vibrations becomes noticeable in the flux-jump region); (ii) Each $J_c(B_a)$ curve measured with significant frequency exhibits two kinks at fields above 3 T (best seen from the curve measured with $f = 40$ Hz and $A = 1$ mm); (iii) The positions of the kinks on the $B_a - J_c$ axes depend on frequency and amplitude of the vibrations in a similar fashion as for YBCO films; (iv) The variation of $J_c(B_a)$ by frequency

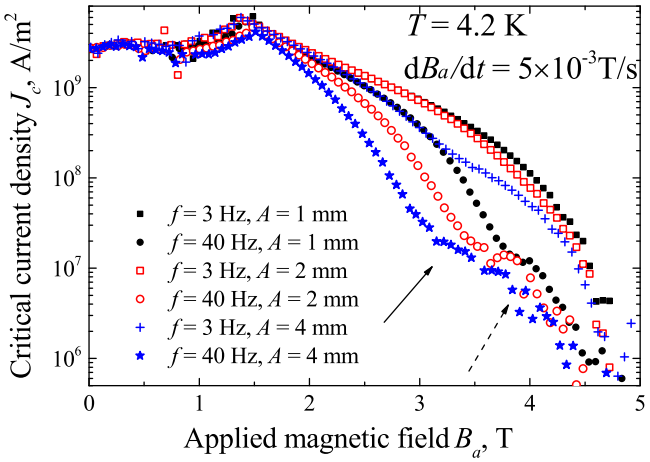

Figure 2. Critical current density dependence on magnetic field of Nb-1 thin film at $T = 4.2$ K measured at $dB_a/dt = 5 \times 10^{-3}$ T s^{-1} with different f and A.

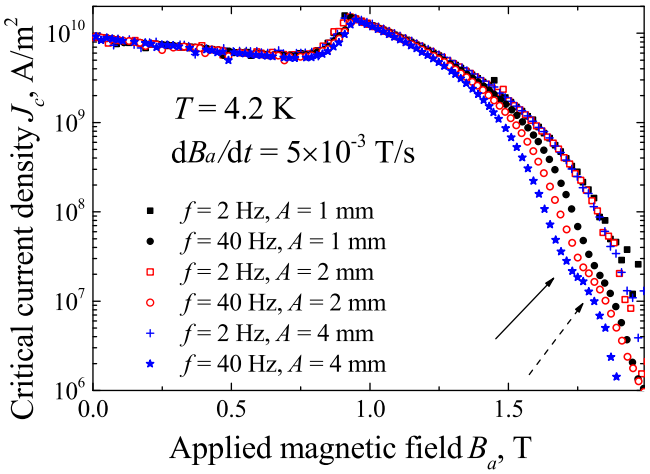

Figure 3. Critical current density dependence on field of Nb-2 thin film at $T = 4.2$ K measured at $dB/dt = 5 \times 10^{-3}$ T s^{-1} with different f and A.

has the same behavior as in the YBCO film (i.e. J_c degrades rapidly with f at low frequencies and then will bunch up at higher frequencies); (v) The maximum reduction of J_c relative to the *undisturbed* state induced by vibrations is of ~40 and observed just above the first kink.

In figure 3, the $J_c(B_a)$ curves for Nb-2 film measured in VSM at different f and A are shown. The microstructure in the Nb-2 film is more ordered (crystalized) than that in the Nb-1 film since the deposition of Nb-2 was performed at the higher temperature, which is above Nb bulk recrystallization temperature. More ordered microstructure provides weaker pinning strength, which is reflected in smaller irreversibility fields by a factor of ~2.5 for Nb-2 than that for Nb-1 (figure 3 versus figure 2). Also, the transparency for the current flow is higher for the Nb-2 film (indicating less defective structure) as can be seen from the larger J_c values at low fields (<1.5 T) as well as from higher T_c.

The general features of the vibration effect in the Nb-2 film is similar to those in the Nb-1 film. However, they are

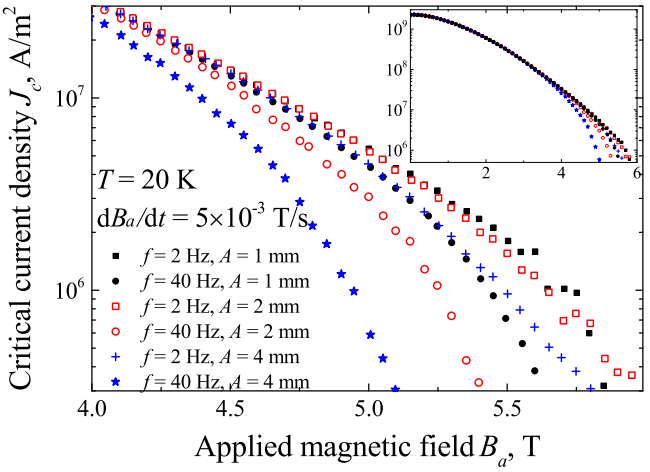

Figure 4. Critical current density dependence on magnetic field of bulk MgB_2 at $T = 20$ K measured at $dB_a/dt = 5 \times 10^{-3}$ T s^{-1} and different f and A. The inset shows the entire critical current density dependence on magnetic field.

less pronounced, in particular in the regions governed by the supercurrent transparency (low fields) rather than pinning (higher fields). The effect of vibrations is only marginal in the flux-jump region of $J_c(B_a)$ and immediately above the peak marking the flux-jump offset in the Nb-2 films. The maximal J_c degradation produced by higher f or/and A is about a factor of 10 in the Nb-2 film estimated at $B_a \simeq 1.7$ T, compared to 40 in Nb-1 as estimated at $B_a \simeq 3$ T (figures 2 and 3). Thus, the vibration effect indicates a strong dependence on material properties.

3.2. Bulk samples

In figure 4, $J_c(B_a)$ measured with different vibration settings are shown for MgB_2 bulk superconductor at $T = 20$ K. At this temperature flux-jumps are not observed in the MgB_2 superconductor [33]. A strong impact of vibrations on the critical current density in the MgB_2 bulk is obvious. As in the case of the thin films, $J_c(B_a)$ does degrade with increasing f and A. In contrast, this degradation occurs at much higher fields ($B_a > 3.5$ T), where $J_c(B_a)/J_c(0) \sim 10^{-2}$ (see the insert in figure 4). In addition, $J_c(B_a)$ exhibits only one weakly pronounced kink, indicating differences in vortex dynamics for thin film and bulk samples.

In figure 5, the $J_c(B_a)$ curves measured at different vibration parameters are shown for the Nb bulk superconductor at $T = 4.2$ K. The behavior of $J_c(B_a)$ somewhat resembles that of the MgB_2 bulk sample, despite the much lower irreversibility field and different material (pinning) properties: (i) The vibration effect starts to show up at relatively high magnetic fields ($B_a > 0.55$ T) at which $J_c(B_a)/J_c(0) \lesssim 10^{-2}$ (this field region is also above the flux-jump region); (ii) The $J_c(B_a)$ curves progressively degrade more rapidly with increasing frequency; (iii) Only one kink's features are observed (in contrast to the thin films), which notably develops at high frequencies.

Summarizing, the vibrations affect J_c of very different types of superconductors at all temperatures, and $J_c(B_a)$ degrades with increasing f and A. The difference between the

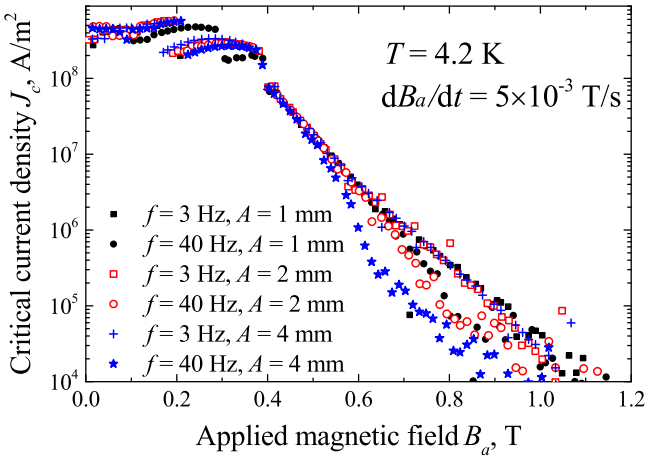

Figure 5. Critical current density dependence on magnetic field of bulk Nb at $T = 4.2$ K measured at $dB/dt = 5 \times 10^{-3}$ T s^{-1} and different f and A.

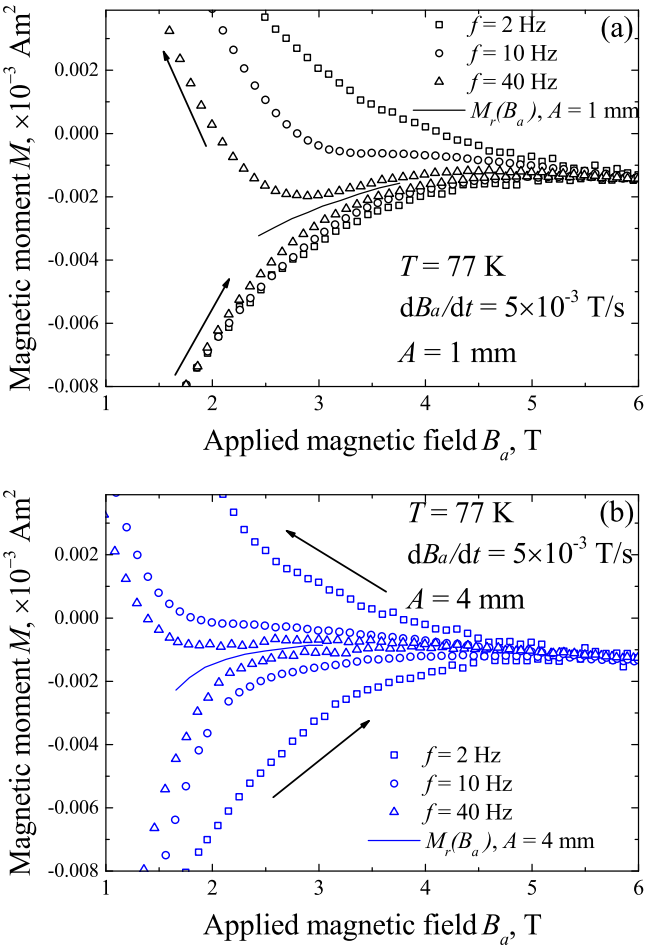

Figure 6. Magnetic moment dependence on magnetic field of YBCO thin film at $T = 77$ K measured at $dB_a/dt = 5 \times 10^{-3}$ T s^{-1} from FC state with varied f and fixed $A = 1$ mm (a) and $A = 4$ mm (b). Arrows show directions of magnetic field sweep. Hypothetical reversible magnetizations M_r are shown with solid lines.

different types of superconductors measured can empirically be ascribed to the differences in the geometrical factors (thin films versus bulk), rather than the type of superconductors (conventional superconductors, high temperature superconductors or MgB_2), keeping in mind that the thin film forms possess different pinning mechanisms compared to the bulk counterparts.

The differences induced by the vibrations to the $J_c(B_a)$ behavior in the thin films and bulk superconductors are: (a) The magnitude of degradation in the bulk is smaller; (b) The onset field of the $J_c(B_a)$ degradation is substantially larger; (c) The kink behavior is less pronounced in bulk with no second (high-field) kink observed.

The observation of these differences suggests that the influence of the vibrations is less pronounced in the samples with stronger measurement signals. It is simply because the signal to the vibration influence ratio is larger, hence larger signals are less sensitive to the features induced by the vibrations. Thus, the samples with larger volumes, such as bulk samples, would naturally have larger signals upon magnetization measurements. Note this preliminary conclusion has nothing to do with the quality of the samples, pinning strength, and the largeness of J_c in the samples. Therefore, to maximise the focus on the influence of the vibrations on the $J_c(B_a)$ behavior, in the following we should mainly deal with YBCO thin films producing the most pronounced features induced by the vibrations. Although the origin of the vibration influence is presumably similar in different types of superconductors, the differences in its appearance are likely due to different features of vortex pinning and dynamics (including geometrical) in these superconductors.

4. Influence of vibrations on the magnetization of YBCO thin films

In figures 6 and 8, a part of the magnetization loops ($M(B_a) = m(B_a)V$, where V is the sample volume used for the calculations of $J_c(B_a)$ in figure 1 and m is a specific magnetization) is shown in the proximity of the irreversibility field (the field at which the irreversible magnetization becomes reversible). All hysteresis loops have some asymmetry between ascending and descending magnetization branches established by the Meissner effect (the field sweep directions are shown by the arrows). This asymmetry is the most pronounced for magnetization measured with high frequency (the best seen in figure 6(a) for the curve measured with $f = 40$ Hz and $A = 1$ mm). Another common feature of all magnetization curves in figures 6 and 8 is the small negative slope visible for the reversible part of the $M(B_a)$ curve produced by the diamagnetic $SrTiO_3$ substrate.

In figure 6(a), the vibration amplitude is fixed at $A = 1$ mm. The influence of the frequency of the vibrations on the magnetization is significantly stronger for the descending branches. Upon increasing f, the magnetization loop 'shrinks' closer, approaching to the reversible section of the loop $M_r(B_a)$ determined by the Meissner effect and schematically indicated in figure 6(a) by the solid line. The reversible magnetization $M_r(B_a)$ in hard superconductors at fields much higher than the

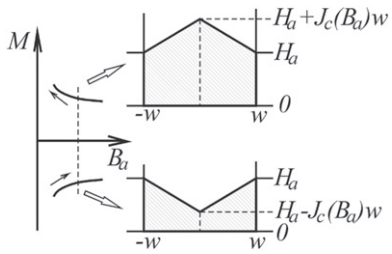

Figure 7. Schematic distribution of magnetic flux in ascending and descending magnetic field at the same B_a within the Bean model.

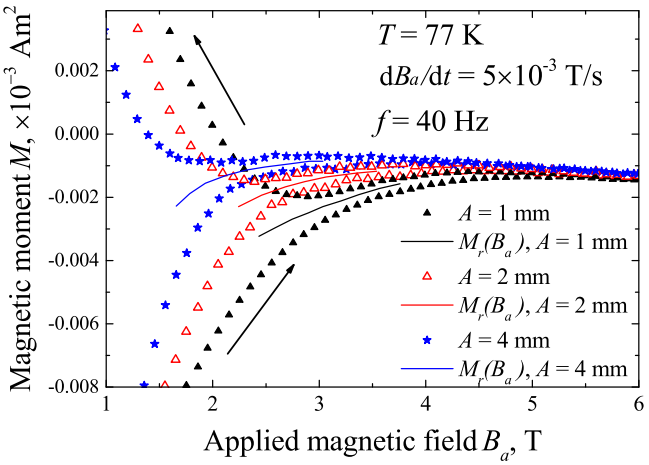

Figure 8. Magnetic moment dependence on magnetic field of YBCO thin film at $T = 77$ K measured at $dB_a/dt = 5 \times 10^{-3}$ T s^{-1} from FC state with $f = 40$ Hz and different A. The arrows show the directions of the magnetic field sweep. The reversible magnetizations M_r are schematically shown by the solid lines.

full penetration field is known to be in the middle between ascending and descending field branches [8, 34].

Thus, we have estimated $M_r(B_a)$ as the average of both magnetization branches measured at the highest f. The 'shrinkage' of $M(B_a)$ to $M_r(B_a)$ occurs mainly due to changes in the descending magnetization branch.

The asymmetrical influence of the increasing frequency of the vibrations on the descending and ascending magnetization branches can indicate a difference in the free energy of the vortex lattice structure in the branches as follows. It is known that well above the full penetration field (assuming the absence of surface barriers and Meissner state), the slope of the distribution of magnetic flux in the superconductor does not depend on the magnetic field sweep direction and is defined completely by circulating critical current $J_c(B_a)$ [35, 36]. The distribution of the magnetic flux in a superconducting strip of $2w$ wide within the Bean model is shown schematically in figure 7 for the ascending and descending magnetization branches. The free energy of the superconductor can be represented in the London fashion as:

$$F = F_0 + \int (\alpha J_c^2 + \vec{B}_a \vec{H}/2) \mathrm{d}V \qquad (1)$$

where the first integrand term (αJ_c^2) is the total kinetic energy of the supercurrent with α being the parameter relevant to the superconducting material, and the second integrand term is the magnetic energy. Considering the critical state model (figure 7), the first term is the same in both ascending and descending B_a, while the second term is higher in descending field as follows from figure 7. Hence, the thermodynamical stimulus towards the minimum energy (uniform flux distribution across the sample and suppressed current) is stronger in descending magnetic field due to the enhanced free energy.

Another possibility for the asymmetry of the magnetization response to the frequency of the vibrations is dependence of pinning strength on the ordering of the vortex lattice. More ordered flux line lattices have smaller total pinning energy [37–40]. At certain magnetic field, the flux line lattice (FLL) is less ordered in increasing magnetic field [37, 38] because when flux penetrates the superconductor it 'injects' some disorder into the lattice [39, 40]. Hence, the vibrations might have a stronger effect on the FLL in decreasing fields due to reduced pinning efficiency.

Figure 6(b) shows magnetization hysteresis loops measured with the larger $A = 4$ mm at different f. In this case, the influence of the frequency on $M(B_a)$ is similarly substantial for ascending and descending field branches, although the certain asymmetry between the branches due to the influence of the frequency change is still observed. The maximum deviation of M induced by vibrations in ascending magnetic field is more than a factor of 2 larger than in the descending magnetic field at $B_a \simeq 1.7$ T. Apparently, the vibrations with larger amplitudes provide significantly stronger drives for vortex structures, and promote the effective redistribution of these structures towards the equilibrium even in the ascending magnetic field. Upon increasing f, the magnetization loops also 'shrink' to a reversible $M_r(B_a)$ (schematically shown as a solid line in figure 6(b)).

Figure 8 shows the hysteresis loops measured with $f = 40$ Hz and different A, while the reversible $M_r(B_a)$ are schematically shown by the solid lines. The influence of the vibration effect with the increasing A on M appears as follows: (i) The irreversibility onset shifts to lower applied magnetic fields, in accordance with the J_c dependence on the vibration parameters obtained in figure 1; (ii) The irreversibility degrades more rapidly to the reversible behavior at larger amplitudes; (iii) The reversible magnetization $M_r(B_a)$ is reduced. The suppression of $M_r(B_a)$ indicates the increased penetration depth λ, which grows with temperature. Thus, the $M_r(B_a)$ shift at a high f in increasing A can only imply the generation of additional heat induced by these vibrations with large amplitude.

In contrast, no heating related effects are observed for the vibration with $A = 1$ mm at any frequency (figure 6(a)). For this amplitude, the changes in the M loops may only imply the increase of temperature in decreasing f, which is not plausible.

4.1. Influence of vibrations on the relaxation of magnetization

The relaxation of magnetization in superconductors is typically measured by VSM or SQUID magnetometer, and occurs due to the thermally activated redistribution of magnetic flux

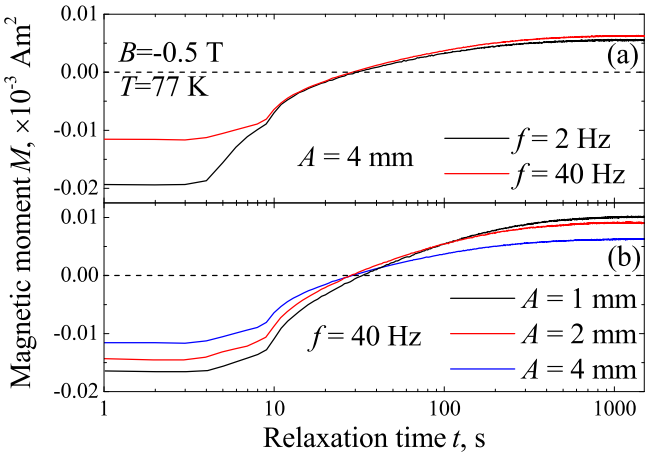

Figure 9. The time dependence of magnetization measured at $T = 77$ K and $B_a = -0.5$ T with $A = 4$ mm and different f (a), and with $f = 40$ Hz and different A(b).

towards uniform distribution [41]. The relaxation is particularly large in high temperature superconductors due to their small coherence length (thus, low vortex pinning barrier) and strong thermal activations [42, 43].

Within Kim–Anderson linear approximation for pinning energy barrier and Arrhenius depinning probability [43–46], the current (magnetization) at a fixed magnetic field decays with time logarithmically [41]:

$$J(t) = J_{c0}\left(1 - \frac{kT}{U}\ln\left(\frac{t}{t_0}\right)\right) \tag{2}$$

where $J(t)$ is current in superconducting film, kT is a thermal energy, U is a vortex pinning barrier (for the YBCO thin films grown by PLD, U is given by equation (4) in [18]), t_0 is an 'effective' hoping attempt time ($t_0 = 1/\nu_0$ in [18]).

In figure 9, the magnetization decay in YBCO thin film with time is shown at $T = 77$ K and $B_a = -0.5$ T. Before these relaxation measurements the sample was field-cooled at $B_a = -8$ T and then the magnetic field was set at the measurement field in the so-called no-overshoot mode. The VSM measurements were performed during the entire magnetic field sweep process in order to capture the very beginning of relaxation process. VSM requires several seconds for acceleration to reach the set values of f and A during this acceleration time certain relaxation occurs. Thus, these few seconds at the beginning of the relaxation, the magnetization might be affected.

A magnetic field of -0.5 T was chosen for the measurements due to several reasons: (i) The vibration effect on magnetization is significantly stronger in descending magnetic field than in ascending field (see for example figure 6); (ii) The effect also becomes obvious in YBCO films when magnetic field $|B_a| > 0.5$ T (figure 1), but when $|B_a|$ exceeds 1 T the dipole moment drops substantially affecting reliability of the measurement; (iii) The measurements of magnetic moment in increasing $|B_a|$ is noisier in the positive region of $0.2 < B_a < 1.2$ and can affect the reliability.

The plateau observed at the beginning of the relaxation process in figure 9 might be due to the no-overshoot mode of setting the magnetic field (progressive deceleration of the field sweep rate upon approaching the set point). This plateau has been referred to some initial relaxation driven redistribution of the magnetic flux [47]. After the plateau, the magnetic moment decreases for all the measurement settings (figure 9) as expected and as anticipated from the J_c dependence on the vibration settings (figure 1). The relaxation process of flux redistribution shows only marginal changes at $t > 1000$ s. The final vortex ordering depends on the vibration amplitude (figure 9(b)), while the frequency dependence is weak (figure 9(a)). This dependence can result from the different thermal response to the vibration at high f and A (as discussed above). Furthermore, note that the magnetization measured crosses $M = 0$ during the relaxation process, whereas it should be expected to stop (to level) once the reversible magnetization $M_r(B_a)$ is reached. Hence, it further indicates that the concept presented in the previous section (figures 6 and 8) that the reversible (Meissner) magnetization $M_r(B_a)$, being sensitive to temperature, is defined by vibration amplitude A (figure 9(b)).

In order to compare the relaxations of magnetization in figure 9, which start and end at various values of M, the normalized rate S of relaxation has been calculated. The S can be derived from the equation (2) as follows:

$$S = \frac{1}{M(t)}\frac{\mathrm{d}M}{\mathrm{d}\ln t} = \frac{\mathrm{d}\ln M}{\mathrm{d}\ln t} = -\frac{kT}{U} \tag{3}$$

where M is the normalized magnetization measured. As can be noted from equation (3), the value of $-1/S$ gives the pinning potential barrier U. In figure 10, the pinning potentials derived from the normalized relaxation are plotted. Thus, the pinning energy decreases due to vibration of the YBCO film. The degradation of U is enhanced if both frequency and amplitude is increased. The vertical segments of the $U(M)$ curves (in figure 10) are the consequence of the constant magnetizations at the beginning of relaxation (figure 9).

In general, at constant magnetic field pinning energy U depends on temperature T, density of pinning centers, pinning energy of single pinning site U_0 [18] and on the ordering of the vortex lattice [39]. Thus, the degradation of U induced by the sample vibration can be interpreted in several ways as follows: (i) The increase of effective temperature due to corresponding FLL vibrations; (ii) The sample vibration drives the vortex lattice into a metastable pinning state with, for example, more ordered FLL [39], which is less adapted to the pinning landscape. It also may partly be the consequence of (i); (iii) The effective degradation of pinning strength of single dislocation, which may also be the consequence of (i) and (ii).

5. Scaling of $J_c(B_a)$ by the interplay between magnetic field sweep rate and frequency

Above, we have shown that the thermal response of YBCO film to vibration with high A and f plays an important role,

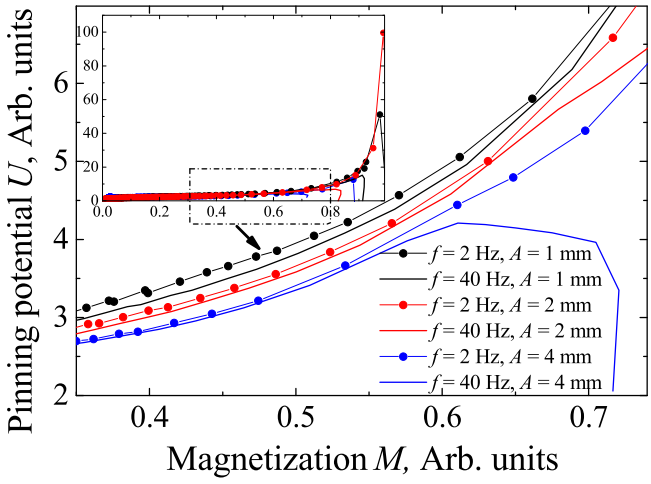

Figure 10. Pinning potential dependence on magnetization (current) during relaxation of magnetization at $T = 77$ K and $B_a = -0.5$ T, obtained from normalized magnetization in figure 9 employing equation (3).

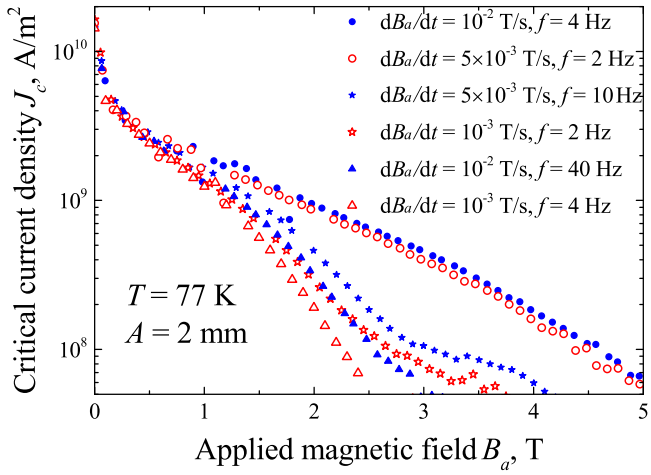

Figure 11. Three pairs of the *scaled* critical current density dependences for which the ratios between the sweep rates (dB_a/dt) is the same as that between the scaling frequencies (f) measured at $A = 2$ mm and $T = 77$ K.

while it is marginal for vibration with low A. Thus, another mechanism suppressing J_c upon vibration of a superconductor should exist, which may be associated with a certain perturbation of vortex dynamics. If this is the case, the vibration effect should be sensitive to the velocity of vortex motion ($\langle v\rangle$), i.e. the effect of vibration on J_c should be scalable with the ratio of $\langle v\rangle/f$.

In figure 11, the $J_c(B_a)$ dependences measured with the amplitude of $A = 2$ mm (exhibiting an insignificant heating effect) at $T = 77$ K are shown for different ratios $\langle v\rangle/f$. Since the velocity of vortex motion $\langle v\rangle$ is proportional to the magnetic field sweep rate dB_a/dt, [18, 21] we use the employed sweep rates as a vortex velocity measure. According to our hypothesis, if we use two different sweep rates, we should be able to scale $J_c(B_a)$ curves with different frequencies. Indeed, the scaling works as can be seen for the three different pairs of the $J_c(B_a)$ dependences for which the ratios between the sweep rates is the same as that between the scaling frequencies (figure 11). The pairs of the dependences are plotted as follows: one curve with solid symbols and the other with the same open symbols for the sweep and frequencies ratios between the pairs equal to 2 (circles), 5(stars), and 10 (triangles). The so-plotted pairs of scaled curves nearly coincide or closely follow each other behaviour. Indeed, according to the irreversibility field dependence on the electric field criteria (figure 2 in [18]) the difference between the curves measured with $dB_a/dt = 10^{-2}$ T/s and $dB_a/dt = 5 \times 10^{-3}$ T/s (the dB_a/dt ratio of 2) should be ~0.2 T, while corresponding reduction of VSM frequency by factor of 2 makes these curves almost coincide. The example of curves with the dB_a/dt ratio of 10 ($dB_a/dt = 10^{-2}$ T/s and $dB_a/dt = 10^{-3}$ T/s) is even more spectacular. The expected difference between these sweep rates in B_{irr} (figure 2 in [18]) is >1 T, while the difference scaled by the frequencies is <0.4 T. Moreover, in addition to the irreversibility field scaling, the pair (plotted by stars) measured for the dB_a/dt ratio of 5 ($dB_a/dt = 5 \times 10^{-3}$ T s^{-1} and $dB_a/dt = 10^{-3}$ T s^{-1}) demonstrates the reasonable reproducibility of the kink-features in $J_c(B_a)$ behaviour. Thus, the obvious interplay between the vortex motion and the frequency as two independently engaged parameters, which enables the scaling of $J_c(B_a)$, is a strong evidence that the vibration with fixed amplitude influences vortex dynamics directly rather than via induced heating (J_c suppression).

6. Vibration effect influence on the irreversibility field

In the previous section, we mentioned the influence of the magnetic field sweep rate (and the corresponding electric field criterion) on the $J_c(B_a)$ dependence and correspondingly on the irreversibility field [18, 21]. The irreversibility field (B_{irr}) is defined at the point on the hysteresis loops where the hysteresis behaviour becomes reversible before reaching the upper critical field (B_{c2}). For our YBCO thin films, $B_{irr} \sim 5.8 \pm 0.2$ T at $T = 77$ K (figure 1). It demonstrates only a weak dependence on the vibration parameters that can be attributed to the sample heating induced by vibrations at high f and A. However, the $J_c(B_a)$ behaviour is strongly dependent on the frequency and amplitude (figure 1) in particular at $B_a > 1$ T and $f > 1$ Hz, the behaviour becomes quite complex. Quantitative models for $J_c(B_a)$ that employ B_{irr} for fitting $J_c(B_a)$ curves [19, 31] or pinning force through Kramer plots in YBCO [48–50] and MgB_2 [51, 52] do not take into account vibrations, and hence cannot explain the kinks in the $J_c(B_a)$ behaviour nor the B_{irr} variations.

Using our model (equation (6) in [18]), we have fitted the low field parts (up to 3T) of these curves (before the kink at $B_a \sim 3$ T) to obtain the set of J_c curves as if there was no kink at ~3 T. The kink may indicate a vortex lattice or vortex pinning related transition. Then, the B^*_{irr} has been defined at the intersection of these fitting curves with the line $J = 5 \times 10^7$ A m^{-2}. Note that the so-defined B^*_{irr} is well suitable for fitting $J_c(B_a)$ curves in YBCO films as shown in [19, 31] or for fitting pinning force through Kramer plots [48–50].

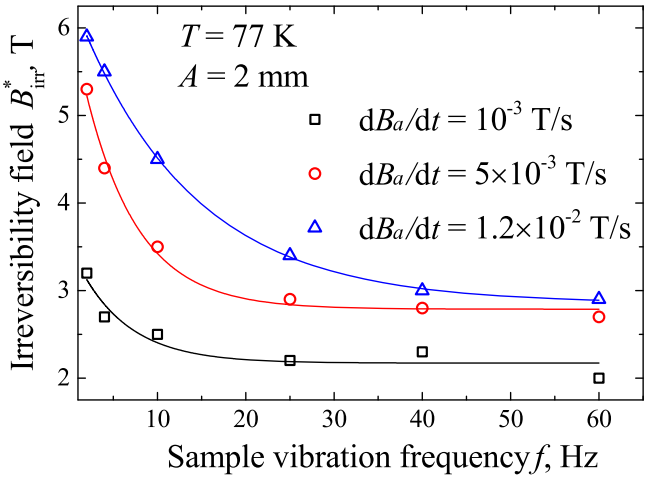

Figure 12. The dependence of the irreversibility field on the frequency at $T = 77$ K for three different magnetic field sweep rates.

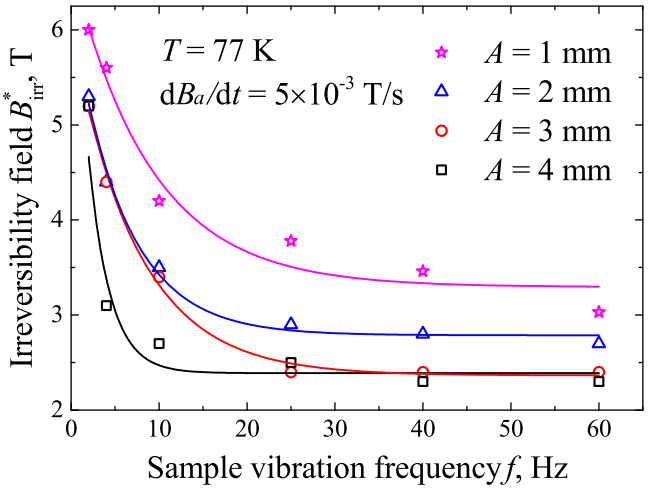

Figure 13. Irreversibility field dependence on frequency at $T = 77$ K measured at four different VSM amplitudes.

Table 1. Parameters for equation (4) used to fit the experimental data in figure 12.

dB_a/dt, $\times 10^{-2}$ T/s	B_{irr}^T, T	B_{irr}^f, T	f_d Hz
0.1	2.17	1.36	5.6
0.5	2.79	3.41	6.0
1.2	2.85	3.56	13.1

In figure 12, the so-obtained B_{irr}^* is plotted as function of the measurement frequency for three different magnetic field sweep rates with the fixed amplitude of 2 mm to rule out the thermal effect induced by vibrations. Hence, figure 12 mostly illustrates the impact of vibration frequency on dynamics of the vortex lattice. In general, it appears that B_{irr}^* decreases logarithmically with the frequency increase. The data can be fitted with the following expression:

$$B_{irr}^*(f) = B_{irr}^T + B_{irr}^f \exp(-f/f_d), \quad (4)$$

where B_{irr}^T is the tempered value of the irreversibility field measured at high frequencies, B_{irr}^f is the value of the irreversibility field drop due to vibration at the highest frequency, f_d is a characteristic frequency of the irreversibility field decay, $[B_{irr}^T + B_{irr}^f]$ is the irreversibility field of 'undisturbed' superconducting sample, measured at $f \to 0$ Hz. Fitting parameters are shown in table 1.

Figure 12 and equation (4) illustrate the scaling of $J_c(B_a)$ by the ratio $\langle v \rangle / f$ discussed in section 5. Indeed, the characteristic frequency f_d increases with increasing dB_a/dt (table 1), showing the interdependent dependence of these parameters on the reduction of $B_{irr}^*(f)$. This is exactly what is predicted by the J_c scaling with the ratio $\langle v \rangle / f$: B_{irr}^* is reduced relative to $B_{irr}^*(f = 0)$ at smaller frequency for slower vortices (lower dB_a/dt).

In figure 13, B_{irr}^* reflecting the J_c behaviour is plotted as a function of frequency for a fixed dB_a/dt and four different amplitudes. As the amplitude of vibrations is increased the $B_{irr}^*(f)$ curves shift to lower values. By fitting the plotted data with the same expression (equation (4)), the following fitting parameters are given in table 2.

Table 2. Parameters for equation (4) used to fit the experimental data in figure 12(b).

A, mm	B_{irr}^T, T	B_{irr}^f, T	f_d Hz
1	3.29	3.41	9.0
2	2.79	3.41	6.0
3	2.36	3.65	7.4
4	2.39	5.21	2.4

One would expect that all $B_{irr}^*(f)$ curves obtained with constant dB_a/dt should have the same $B_{irr}^*(f \to 0) = B_{irr}$ for different vibration amplitudes. However, the superconductor may be very sensitive to thermal effects arising from increasing the amplitude, which leads to a similar behaviour to that induced by faster moving vortices at larger dB_a/dt. Notably, the characteristic frequency f_d does not decrease consistently with increased amplitude (table 2), which may also indicate that the reduction of $B_{irr}^*(f)$ in increasing amplitude is driven not only by the vortex dynamics, but also by thermal effects.

7. Possible origin of vibration-induced phenomena

In order to suppress the magnetization (critical current density), the vibrations of superconductors need to induce some propagation of vortex lattice perturbations during VSM experiments. The most straightforward source of such propagation would be inhomogeneities in the experimental environment or conditions, which are nominally assumed to be constant. All inhomogeneities in the measurement environment can be divided into thermal and magnetic fluctuations. There are two possibilities for thermal perturbations: (i) The actual inhomogeneity of

temperature in the sample's space and (ii) Bardeen-Stephen heating caused by periodic vortex motion [53] (if we assume that this motion is induced by vibrations). Any vibration-induced heating would lead to the degradation of the pinning potential, which is proportional to the density of moving vortices (i.e. B_a) and vibration frequency. The evidence for the thermal response of the sample to the vibrations with high amplitudes has been demonstrated in terms of reduction of Meissner current in figures 8 and 9.

Temperature dependence of $B_{\rm irr}$ was shown to be [54, 55]:

$$B_{\rm irr}(T) = B_{\rm irr}(0)(1 - T/T_c)^n, \quad (5)$$

where $n \simeq 3/2$ [42, 56], $B_{\rm irr}(0)$ is the irreversibility field at zero temperature. Equation (5) can be used for estimations of temperature increase due to vibration, employing the $B^*_{\rm irr}$ dependences (figures 12 and 13). For example, we can assume that the entire degradation of $B^*_{\rm irr}$ from its value of $\simeq$6 T at $f \to 0$ and $A = 1$ mm (figure 13) to $B^*_{\rm irr} \simeq 2.5$ T at $f > 25$ Hz and $A = 4$ mm as a result of vibration is caused by the temperature increase. In this case, according to equation (5), the maximum temperature rise would be more than 5 K. Such significant temperature change should have been easily detected by the PPMS thermometer. However, the temperature was stable throughout the measurements. This is an additional proof that the critical current density degradation due to vibrations is not governed only by temperature effects.

Furthermore, we have discussed in the preceding sections that no signature of any thermal influence resulted from vibration with $A = 1$ mm. Obviously, the vibrations at $A = 1$ mm with increasing frequency lead to the reduction of $B^*_{\rm irr}$ from 6 T to 3.5 T (figure 13). Thus, the heating may be considered responsible for $B^*_{\rm irr}$ decrease from 3.5 T to 2.5 T (at $f > 25$ Hz) if the amplitude is increased to 4 mm. In this case, the temperature rise due to vibrations estimated with equation (5) would not exceed ~1 K, which is also significant overestimation as this $B^*_{\rm irr}$ degradation is also driven by vortex dynamics. If we further assume that the heating effect is responsible for the 50% of the $B^*_{\rm irr}$ degradation (i.e. ~0.5 T, being also the uncertainty in the *measured* $B^*_{\rm irr}$ seen in figure 1), then the estimation of the temperature rise with equation (5) gives only the tenth part of Kelvin.

This above analysis shows that the sample vibration can generate a certain heating effect, but the J_c (and corresponding $B^*_{\rm irr}$ degradation associated with it is expected to be relatively small. Hence, the magnetic perturbations (driving vortex motion) demonstrated in figure 11 play a major role in the sample vibrations measured by VSM. There are at least three sources of small magnetic field perturbations, which can arise during PPMS VSM measurements: (i) Inhomogeneities of the magnetic field along the axis of the magnet (z-axis), thus any movement of the superconductor along the z-axis (VSM oscillations) would expose the superconductor to the field inhomogeneities (e.g. [16]); (ii) Inhomogeneities of the magnetic field in the plane perpendicular to the z-axis (across the bore of the magnet), hence any displacement from the perfect z-axis movement would be felt by the superconductor; (iii) Tilting of the superconductor relative to external magnetic field (as for the vibrating reed experiments [13, 57]. The first two reasons are the consequences of the geometry of the PPMS superconducting magnets, whereas the third reason might arise due to various mechanical imperfections of the vibration mechanism.

In general, periodic movement of a superconductor in an inhomogeneous magnetic field causes redistribution of vortices due to generated ac supercurrents [13]. These supercurrents depend on the level of field inhomogeneities and the amplitude of the oscillations. In the case of the tilting of the superconductor relative to the z-axis, this process reminds the so-called flux line walking described in [7] and observed in [8–10]. The small in-plane periodic field is considered to 'shake' vortices out of pinning centers and force their relaxation [7, 11, 12]. A small ac current is induced by the in-plane magnetic field oscillations (resulting from the deviation of the magnetic field direction from the sample's z-axis) tends to tilt vortices at each cycle of the oscillations, so that FLL is forced into more equilibrium position decreasing $\vec{\nabla} \times \vec{\mathbf{B}}$. If the frequency of oscillations would increase, it leads to more periods of relaxation happening over the same period of time and hence to a stronger decrease in magnetization (J_c) and $B^*_{\rm irr}$. Qualitatively, it agrees with the reduction of the irreversible magnetization and the drop of the critical current density observed in [56]. This shaking process reminds our experiments in VSM. However, in our case the frequency range is more than an order of magnitude lower, as well as the frequency increase reduces the irreversibility field to a certain constant value $B^T_{\rm irr}$ (equation (4)), while in the shaking process the irreversibility field can be suppressed completely [8].

8. Conclusion

In this work an effect of vibration on the magnetization, critical current density and irreversibility field of superconductors was studied during VSM experiments. It was shown that the vibration affects J_c of all possible types of superconductors during their VSM measurements. Increasing vibration frequency and/or amplitude leads to progressive reduction of the critical current density as the function of the applied magnetic field. Results obtained for different bulk materials and thin films can be summarized as follows: (i) The vibration of the superconductor affects the critical current density of superconducting samples regardless of the geometry of the sample, vortex pinning properties or measurement temperature, the effect develops in increasing B_a; (ii) The vibration effect is more intense in thin films, it starts to take place at smaller B_a and higher J_c than in bulk superconductors; (iii) Vibrations develop two kinks on $J_c(B_a)$ curves in the thin films and only one rather weak kink in the bulk samples, indicating certain transitions in vortex state/motion. The kinks become more pronounced by enhancing f and/or A; (iv) Different trends of the $J_c(B_a)$ behavior to the variation of vibration frequency are revealed for bulk materials and thin films: in bulk materials, the $J_c(B_a)$ curves progressively degrade with increasing f faster than in the thin films, in which the $J_c(B_a)$ curves degrade rapidly at low f and

then remain unchanged at higher f; (v) The vibration of superconductors affects the flux-jumps process during magnetization measurement.

Analysis of magnetization curves measured for the YBCO thin films has shown that the responses of magnetization to changes in frequency and amplitude are qualitatively different. The study of magnetization dependence on the applied magnetic field measured at different vibration parameters revealed the asymmetry of the vibration effect on ascending and descending magnetic field branches. This indicates different states of vortex lattice in these two branches. A frequency increase leads to the emergence of a certain reversible (Meissner-like) state with its own $M_r(B_a)$ dependence. The emergence of the reversible state from irreversible hysteresis loops is significantly faster if the vibrations possess large amplitudes. In this case, $M_r(B_a)$ is reduced compared to small amplitudes, indicating certain thermal processes in the superconductor.

Analysis of the relaxation experiments confirmed that increase of the vibration amplitude leads to a certain heating of the superconductor. At large A, heating can increase with increasing f. Relaxation measurements also showed that the effect of vibrations can be thought of as decreasing pinning potential with increasing frequency and/or amplitude (figure 10).

The $J_c(B_a)$ dependences measured with different magnetic field sweep rates were shown to be scalable with the corresponding frequency (figure 11), suggesting that the frequency induces vortex motion. Hence, the vibration effect is likely driven by the vortex dynamic, which is at high f and/or A assisted by thermal effect. This result was further supported by the irreversibility field B^*_{irr} behaviour, which exhibits logarithmic decay in increasing frequency.

Thus, the effect of the vibrations on the critical current density and and irreversibility field is governed by thermal and magnetic perturbations of the vortex structure. The role of heating effect is shown to be relatively small, while magnetic perturbations promote relaxation of the vortex lattice in a sweeping magnetic field, degrading the critical current density in a somewhat similar fashion to vortex shaking [7, 11, 12].

The nature of the kinks in $J_c(B_a)$ behaviour is assumed to be the indication of some dynamic transitions of the vortex lattice, which is currently under investigation.

Acknowledgments

The authors have benefited from fruitful discussions with Tom H Johansen. This work is supported by the Australian Research Council via Discovery Projects (DP110100398), as well as by the Faculty of Engineering and Information Sciences and by AIIM, University of Wollongong. IAG acknowledges the financial support of the Russian Foundation for Basic Research (RFBR) (research project No. 16-32-00309) and of the Ministry of Education and Science of the Russian Federation in the framework of Increase Competitiveness Program of NUST 'MISiS' (research project No. K2-2014-025) at the last stages of this research work.

References

[1] Xu K, Wu X and Pan P 2009 *Appl. Phys. Lett.* **95** 072502
[2] Malozemoff A P, Worthington T K, Yeshurun Y and Holtzberg F 1988 *Phys. Rev.* B **38** 7203
[3] Müller K H 1990 *Physica* C **168** 585
[4] Olsson H K, Koch R H and Robertazzi R P 1991 *Phys. Rev. Lett.* **66** 2661
[5] Owliaei J, Sridhar S and Talvacchio J 1992 *Phys. Rev. Lett.* **69** 3366
[6] Coffey M W and Clem J R 1991 *Phys. Rev. Lett.* **67** 386
[7] Brandt E H and Mikitik G P 2002 *Phys. Rev. Lett.* **89** 027002
[8] Avraham N *et al* 2001 *Nature* **411** 451
[9] Willemin M, Rossel C, Hofer J, Keller H, Erb A and Walker E 1998 *Phys. Rev.* B **58** R5940
[10] LeBlanc M A R, Celebi S and Rezeq M 2001 *Physica* C **361** 251
[11] Mikitik G P and Brandt E H 2004 *Phys. Rev.* B **69** 134521
[12] Brandt E H 1993 *Phys. Rev.* B **48** 6699
[13] Esquinazi P 1991 *J. Low Temp. Phys.* **85** 139
[14] Pan A V, Ziese M, Höhne R, Esquinazi P, Knappe S and Koch R 1998 *Physica* C **301** 72
[15] Pan A V and Esquinazi P 2004 *Phys. Rev.* B **70** 184510
[16] Luzhbin D A, Pan A V, Komashko V A, Flis V S, Pan V M, Dou S X and Esquinazi P 2004 *Phys. Rev.* B **69** 024506
[17] Magnetic Property Measurement System. SQUID VSM Users Manual. Part Number 1500-100, C0, 2009; Physical Property Measurement System. Vibrating Sample Magnetometer (VSM) Option Users Manual. Part Number 1096-100, A3, 2008
[18] Golovchanskiy I A, Pan A V, Shcherbakova O V and Fedoseev S A 2013 *J. Appl. Phys.* **114** 163910
[19] Polat O, Sinclair J W, Zuev Y L, Thompson J R, Christen D K, Cook S W, Kumar D, Chen Y and Selvamanickam V 2011 *Phys. Rev.* B **84** 024519
[20] Zhukov A A *et al* 1993 *Cryogenics* **33** 142
[21] Pan A V, Golovchanskiy I A and Fedoseev S A 2013 *Europhys. Lett.* **103** 17006
[22] Terentiev A N and Kuznetsov A A 1992 *Physica* C **195** 41–6
[23] Gou X F, Zheng X J and Zhou Y H 2006 *IEEE Trans. Appl. Supercond.* **17** 3795
[24] Nakashima H 1994 *IEEE Trans. Magn.* **30** 1572
[25] Hull J R 2000 *Supercond. Sci. Tech.* **13** R1–5
[26] Golovchanskiy I A, Pan A V, Fedoseev S A and Higgins M 2014 *Appl. Surf. Sci.* **311** 549–57
[27] Shcherbakova O V, Pan A V, Wexler D and Dou S X 2007 *IEEE Trans. Appl. Supercond.* **17** 2790
[28] Shcherbakova O V, Pan A V, Wang J L, Shcherbakov A V, Dou S X, Wexler D, Babic E, Jercinovic M and Husnjak O 2008 *Supercond. Sci. Technol.* **21** 015005
[29] Zhou S, Pan A V, Horvat J, Qin M J and Liu H K 2004 *Supercond. Sci. Technol.* **17** S528
[30] Chen D X and Goldfarb R B 1989 *J. Appl. Phys.* **66** 2489
[31] Aytug T *et al* 2006 *Phys. Rev.* B **74** 184505
[32] Hänisch J, Kozlova N, Cai C, Nenkov K, Fuchs G and Holzapfel B 2007 *Supercond. Sci. Technol.* **20** 228–31
[33] Denisov D V, Shantsev D V, Galperin Y M, Choi E M, Lee H S, Lee S I, Bobyl A V, Goa P E, Olsen A A F and Johansen T H 2006 *Phys. Rev. Lett.* **97** 077002
[34] Hecher *et al* 2016 *Supercond. Sci. Technol.* **29** 025004
Brandt E H 1989 *Science* **243** 349–55
[35] Bean C P 1964 *Rev. Mod. Phys.* **36** 31
[36] Reichhardt C, Olson C J, Groth J, Field S and Nori F 1995 *Phys. Rev.* B **52** 10441
[37] Pan A V and Esquinazi P 2000 *Eur. Phys. J.* B **17** 405
[38] Pan A V and Esquinazi P 2000 *Physica* C **341-348** 1187
[39] Marchevsky M, Higgins M J and Bhattacharya S 2001 *Nature* **409** 591

[40] Koshelev A E and Vinokur V M 1994 *Phys. Rev. Lett.* **73** 3580
[41] Yeshurun Y, Malozemoff A P and Shaulov A 1996 *Rev. Mod. Phys.* **68** 911
[42] Yeshurun Y and Malozemoff A P 1988 *Phys. Rev. Lett.* **60** 2202
[43] Dew-Hughes D 1988 *Cryogenics* **28** 674
[44] Anderson P and Kim Y 1964 *Rev. Mod. Phys.* **36** 39
[45] Savvides N 1990 *Physica* C **165** 371
[46] Palstra T M 1989 *Appl. Phys. Lett.* **54** 763
[47] Gurevich A and Kupfer H 1993 *Phys. Rev.* B **48** 6477
[48] Varanasi C V, Barnes P N and Burke J 2007 *Supercond. Sci. Technol.* **20** 1071
[49] Oh S, Choi H, Lee C, Lee S, Yoo J, Youm D, Yamada H and Yamasaki H 2007 *J. Appl. Phys.* **102** 043904
[50] Lu F, Kametani F and Hellstrom E E 2012 *Supercond. Sci. Technol.* **25** 015011
[51] Larbalestier D C *et al* 2001 *Nature* **410** 186
[52] Cooley L, Song X and Larbalestier D C 2003 *IEEE Trans. Appl. Supercond.* **13** 3280
[53] Bardeen J and Stephen M J 1965 *Phys. Rev.* **140** A1197
[54] Tinkham M 1988 *Phys. Rev. Lett.* **61** 1658
[55] Seidler G T, Rosenbaum T F, Heinz D L, Downey J W, Paulikas A P and Veal B W 1991 *Physica* C **183** 333
[56] Schilling A, Ott H R and Wolf T 1992 *Phys. Rev.* B **46** 14253
[57] Pan A V, Ciovacco F, Esquinazi P and Lorenz M 1999 *Phys. Rev.* B **60** 4293